ROYAL SOCIETY
OF CHEMISTRY

PAPER

Large enhancement of ferroelectric polarization in Hf$_{0.5}$Zr$_{0.5}$O$_2$ films by low plasma energy pulsed laser deposition†

Tingfeng Song, Raul Solanas, Mengdi Qian, Ignasi Fina* and Florencio Sánchez ⓘ *

The ferroelectric phase of HfO$_2$ is generally stabilized in polycrystalline films, which typically exhibit the highest polarization when deposited using low oxidizing conditions. In contrast, epitaxial films grown by pulsed laser deposition show low or suppressed polarization if a low oxygen pressure is used. Epitaxial films are essential to better understand physical properties, and obtaining films that have intrinsic polarization is of great importance. In order to advance towards this objective, we have carried out a systematic study of the epitaxial growth of Hf$_{0.5}$Zr$_{0.5}$O$_2$ combining inert Ar gas with oxidizing O$_2$ gas. This allows us to control the oxidizing conditions (through O$_2$ partial pressure) and the energy of the pulsed laser deposition plasma (through the total pressure of O$_2$ and Ar). A pressure of Ar high enough to significantly reduce plasma energy and that of O$_2$ low enough to reduce oxidation conditions are found to allow a large increase in ferroelectric polarization up to about 30 μC cm^{-2}, representing an increase of around 50% compared to films grown by conventional pulsed laser deposition. This simple growth process, with high impact in the development of ferroelectric HfO$_2$, can be also beneficial in the growth of thin films of other materials by pulsed laser deposition.

1. Introduction

The discovery of robust ferroelectricity in a metastable orthorhombic phase of HfO$_2$,[1] a material compatible with CMOS processes, has generated enormous scientific interest and great expectations for commercial applications. HfO$_2$ is monoclinic (paraelectric) in bulk, but an orthorhombic phase (ferroelectric) can be stabilized at room temperature in doped HfO$_2$ thin films.[2,3] The stabilization of this phase has been achieved using different chemical and physical deposition techniques, being atomic layer deposition (ALD) the most widely used among them. The oxidizing conditions during HfO$_2$ growth are crucial to stabilize the ferroelectric phase. Pal et al.[4] observed an increase in ferroelectric polarization with decreasing the duration of the ALD ozone pulses. This also caused a large increase in the leakage current, which pointed to a high concentration of oxygen vacancies. Materano et al.[5] reported a higher amount of orthorhombic phase and larger polarization in HfO$_2$ and Hf$_{0.5}$Zr$_{0.5}$O$_2$ (HZO) films grown by ALD when the O$_3$ dose was

lowered. This dependence is not observed in the case of pure ZrO$_2$ films.[5,6] Among the physical deposition techniques, sputtering is most commonly used to grow polycrystalline doped HfO$_2$ films. The technique is based on an Ar plasma that sputters a solid target, and a mixed O$_2$/Ar atmosphere is typically needed to grow thin films of most oxides. However, the O$_2$ atmosphere does not favor the stabilization of the metastable ferroelectric phase of HfO$_2$, and pure Ar or low O$_2$ flow conditions are needed. For example, HZO films showed the highest polarization when sputtering was carried out under pure Ar.[7] In the case of undoped HfO$_2$ films, sputtering under a low oxygen flow helps to stabilize the orthorhombic phase.[5] Recently, Mittmann et al.[8,9] reported that a high oxygen flow favors the formation of the paraelectric monoclinic phase in the entire composition range of HfO$_2$–ZrO$_2$, and a low flow was needed to suppress the formation of the tetragonal phase. The reported results, as a whole, indicate that HfO$_2$-based polycrystalline films, deposited by chemical or physical methods, present a greater amount of ferroelectric orthorhombic phase when low oxidizing conditions are used.[10,11] The experimental results are in agreement with theoretical calculations of the reduced energy difference between the metastable orthorhombic phase and the stable monoclinic phase when HfO$_2$ contains oxygen vacancies.[12]

Ferroelectric HfO$_2$ epitaxial films are generally grown by pulsed laser deposition (PLD).[13–17] The technique, unlike sputtering, does not require the use of Ar gas and an atmosphere of

Institut de Ciència de Materials de Barcelona (ICMAB-CSIC), Campus UAB, Bellaterra 08193, Barcelona, Spain. E-mail: ifina@icmab.es, fsanchez@icmab.es

† Electronic supplementary information (ESI) available: Sketches of the P_{Ar} and P_{O_2} partial pressures used to grow the films. XRD θ–2θ scans of the series of films. Simulation of Laue oscillations. Thickness and growth rate as a function of P_{Ar}. XRD pole figures. Intensity of the o-(111) reflection, normalized to that of the STO(002) peak. The normalized o-(111) reflection. Leakage–voltage curves of films. See DOI: 10.1039/d1tc05387f

1084 | *J. Mater. Chem. C*, 2022, **10**, 1084–1089

This journal is © The Royal Society of Chemistry 2022

pure O_2 is commonly used. Lyu et al.[16,18] reported the growth window of ferroelectric epitaxial HZO by PLD. HZO crystallizes at temperature and oxygen pressure (P_{O_2}) greater than about 700 °C and 0.02 mbar, respectively.[16] The amount of orthorhombic phase increases with P_{O_2}, the maximum P_{O_2} ranges from 0.08 to 0.2 mbar (the highest pressure used in the experiments).[16] The ferroelectric polarization exhibits the same dependence on P_{O_2}, confirming that a low oxidizing atmosphere during PLD suppresses the formation of the orthorhombic phase. Regarding leakage current, it is important to note that it decreases with increasing ferroelectric polarization. Therefore, the influence of oxidizing conditions in PLD is the opposite to that in chemical methods or sputtering. On the other hand, ferroelectric doped-HfO$_2$ epitaxial films have been also prepared by solid phase epitaxy using sputtering, and the films deposited under pure Ar showed much better ferroelectric properties than the films deposited under a mixed Ar/O$_2$ atmosphere.[19] Therefore, epitaxial and polycrystalline films show the same dependence on oxidizing conditions when the same deposition method is used. Consequently, the inhibition of ferroelectric phase formation under low oxidizing conditions is specific to films grown by the PLD technique.

The oxygen pressure in a PLD process has an obvious effect on the oxidation of the films. It affects the amount of oxygen vacancies and the phase formed in the case of competing valence states (in Fe$_x$O$_y$ films, for example). The oxygen content in the film will depend, besides the oxygen pressure in the PLD chamber, on the substrate temperature because of the high vapor pressure of oxygen. But the oxygen pressure during PLD is also critical because the material ablated with each laser pulse interacts with the oxygen gas.[20,21] The ablated atoms constitute a very high-energy plasma, the so-called PLD plume, which propagates along the normal direction of the target. When the ablation process occurs in the presence of a background gas, the interaction with the gas atoms reduces the kinetic energy of the ablated species. As the background pressure increases, the plasma energy decreases. The plume scattering also causes a decrease in the growth rate and can produce off-stoichiometry in the case of multi-cation films.[22–24] The kinetic energy of the emitted atoms, which also depends on the laser fluence, can reach tens of eV under low pressure conditions.[25] The effect of the high-energy atoms on the film can be dramatic, reducing the crystallization[26,27] and even causing self-sputtering in the film.[28–30] On the other hand, if the ambient pressure is high enough to thermalize the PLD plasma, the crystallinity of the films also degrades.[27] Therefore, the gas (pressure and composition) during PLD needs to be optimized. These effects must be considered, if a low oxygen pressure is used to decrease oxidation conditions, in order to favor the formation of a particular phase.

A method of reducing the plasma energy without increasing the film oxidation is introducing an inert gas during the PLD process. PLD under an inert gas was scarcely done in the past.[28,29,31,32] Recently, it has been used successfully to obtain transparent conducting SrVO$_3$ films without spurious phases.[33,34] An inert gas can be also necessary to deposit oxide films on highly reactive substrates. For example, pure Ar gas was used to grow HZO films on bare Si.[35] Here, we combine O$_2$ and Ar as ambient gas to grow HZO ferroelectric films by PLD under low oxidation conditions and reduced plasma energy. This allows extending the growth window of epitaxial HZO to lower oxygen pressure without epitaxy degradation caused by an excessively energetic plasma. We show that a low plasma energy allows the increase of ferroelectric polarization in epitaxial HZO films by more than 50% with respect to equivalent films prepared by conventional PLD. The polarization values match well with the theoretically calculated polarization for the ferroelectric $Pca2_1$ orthorhombic phase of HfO$_2$. Low plasma energy processes could be also used to prepare conventional (perovskites) or unconventional (as ε-Fe$_2$O$_3$ or Al$_{1-x}$Sc$_x$N) ferroelectrics with improved properties.

2. Experimental

HZO films were grown on SrTiO$_3$(001) (STO) substrates buffered with a La$_{0.67}$Sr$_{0.33}$MnO$_3$ (LSMO) electrode of $\sim$25 nm thickness. The ferroelectric HZO film and the LSMO electrode were deposited via a single process by PLD using a KrF excimer laser. LSMO electrodes were deposited at a substrate temperature of 700 °C under 0.1 mbar of oxygen. HZO films were deposited at 800 °C under an Ar/O$_2$ atmosphere. Three series of films were grown by varying the Ar pressure (P_{Ar}) with fixed O$_2$ pressure (P_{O_2}) values of 0.01 mbar, 0.05 mbar and 0.1 mbar, and four series by varying P_{O_2} with fixed P_{Ar} of 0 mbar, 0.05 mbar, 0.1 mbar and 0.2 mbar. Sketches in Fig. S1 (ESI†) summarize the P_{Ar}/P_{O_2} values in these series. HZO films were deposited with 800 laser pulses, and immediately after growth, the samples were cooled under 0.2 mbar of oxygen. Structural characterization was performed by X-ray diffraction (XRD) using Cu Kα radiation. Circular platinum top electrodes (thickness: 20 nm and diameter: 20 μm) were deposited by dc magnetron sputtering through stencil masks for electrical characterization. Ferroelectric polarization loops at a frequency of 1 kHz and leakage current were measured in the top-bottom configuration (grounding the bottom electrode and biasing the top one) at room temperature using an AixACCT TFAnalyser2000 platform. Maximum electric field before the sample breakdown was applied for all the samples. Leakage contribution to the polarization loops was minimized using dynamic leakage current compensation (DLCC) procedure.

3. Results

Fig. 1a shows the XRD θ–2θ scans of the films deposited under a mixed Ar/O$_2$ atmosphere (partial P_{O_2} = 0.01 mbar is fixed and partial P_{Ar} is varied, thus varying the total atmospheric pressure). The XRD θ–2θ scans are zoomed around the position of the orthorhombic (o)-HZO(111) reflections (wider 2θ range scans of all samples are presented in Fig. S2, ESI†). The film deposited without Ar, i.e. under pure P_{O_2} = 0 mbar (black line), is not crystallized, in agreement with the reported growth
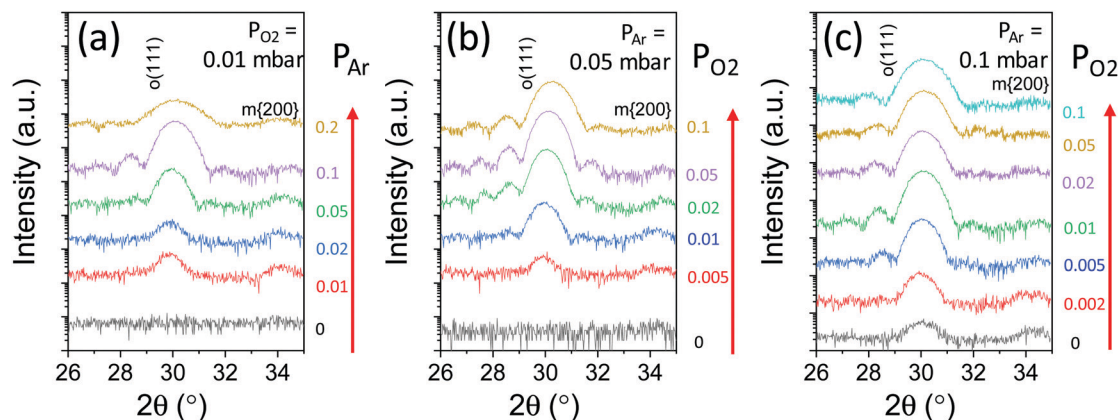
Fig. 1 XRD $\theta-2\theta$ scans of films deposited under a mixed Ar/O$_2$ atmosphere. (a) Fixed P_{O_2} = 0.01 mbar and varying P_{Ar}. The scan corresponding to P_{Ar} = 0 mbar and P_{O_2} = 0.01 mbar has been reported in ref. 16. (b) Fixed P_{Ar} = 0.05 mbar and varying P_{O_2}. (c) Fixed P_{Ar} = 0.1 mbar and varying P_{O_2}.

window for conventional PLD.[16] In contrast, the films deposited under a mixed Ar/O$_2$ atmosphere exhibit a diffraction peak at the position of the o-HZO(111) reflection ($2\theta \sim 30°$) and a less intense peak at $2\theta \sim 34°$ which corresponds to a {200} reflection of the monoclinic (m) phase. The intensity of the o-HZO(111) peak is low in the P_{Ar} = 0.01 mbar and 0.02 mbar samples (red and blue lines, respectively) and high in the P_{Ar} = 0.05 mbar and 0.1 mbar samples (green and purple lines, respectively). Laue oscillations around the o-HZO(111) peak are evident in the P_{Ar} = 0.1 mbar film. The thickness of this film, determined by simulation of the Laue fringes (Fig. S3, ESI†), is 7.7 nm. A higher Ar pressure (0.2 mbar, gold line) results in a less intense and broader o-HZO(111) peak. The width of the peak signals that the film is thinner ($t \sim 5.9$ nm), which is a consequence of the scattering of Hf and Zr atoms by the higher pressure (the dependence of the growth rate with P_{Ar} is shown in Fig. S4, ESI†). In summary, Fig. 1a shows that P_{Ar} = 0.05–0.1 mbar is optimal to stabilize the orthorhombic phase with a very low P_{O_2} of 0.01 mbar. Next, we show in Fig. 1b and c the effect of P_{O_2} when P_{Ar} is fixed at 0.05 mbar and 0.1 mbar, respectively. In the P_{Ar} = 0.05 mbar series (Fig. 1b), the oxygen pressure threshold for crystallization is around $P_{O_2} = 5 \times 10^{-3}$ mbar (red line). The film grown under this P_{O_2} partial pressure shows low intensity o-(111) and m-{200} peaks. The intensity of the o-(111) peak increases notably in the films deposited under higher P_{O_2}, and Laue oscillations are evident in the P_{O_2} = 0.02 and 0.05 mbar films. The pole figures measured in the P_{O_2} = 0.05 mbar film (Fig. S5, ESI†) confirm the epitaxial ordering of the orthorhombic phase. There are twelve poles, signaling the presence of four families of crystal variants, as reported for the equivalent films grown under a pure O$_2$ atmosphere.[14,16] The P_{O_2} = 0.1 mbar film (gold line), which is thinner due to the reduced growth rate caused by plasma scattering, also shows evident Laue fringes. In the P_{Ar} = 0.1 mbar series (Fig. 1c), there is crystallization even in the film deposited without oxygen partial pressure. The XRD scan of the P_{O_2} = 0 mbar film (black line) presents o-(111) and m-{200} diffraction peaks. The intensity of the o-(111) peak increases significantly in the film grown under $P_{O_2} = 2 \times 10^{-3}$ mbar (red line), and it is very intense and

accompanied by Laue fringes in the $P_{O_2} = 5 \times 10^{-3}$ mbar (blue line) and 0.01 mbar (green line) films. The films deposited under higher P_{O_2} are also orthorhombic, and a significant thickness decrease is observed in the P_{O_2} = 0.1 mbar film (turquoise line).

The intensity of the o-(111) reflection allows the quantification of the dependence of the amount of orthorhombic phase on the O$_2$ and Ar partial pressure (Fig. 2). There are no significant differences if normalization is performed with the STO(002) substrate peak (Fig. S6, ESI†). $I_{HZO(111)}/I_{LSMO(002)}$ increases with P_{O_2} (Fig. 2a), with little additional effect of the Ar pressure when P_{O_2} is high. The crystallization is very low in films grown under a pure oxygen pressure lower than 0.05 mbar, but in the presence of additional Ar the stabilization of the orthorhombic phase is greatly enhanced. The amount of orthorhombic phase is slightly underestimated in the two P_{Ar} = 0.2 mbar films due to their lower thickness, but the equivalent graphs normalized to the film thickness exhibit the same relation (Fig. S7, ESI†). The dependence of $I_{HZO(111)}/I_{LSMO(002)}$ on P_{Ar} (Fig. 2b) evidences that, under a high
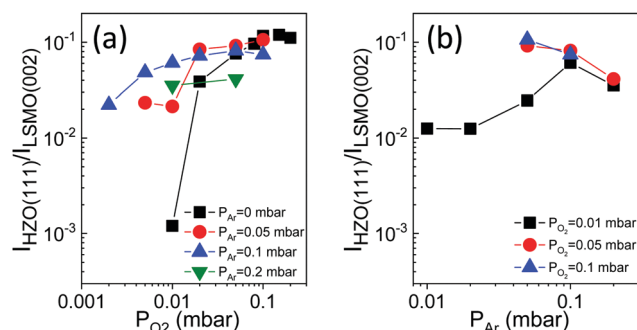

Fig. 2 Intensity of the o-(111) reflection, normalized to that of the LSMO(002) peak, $I_{HZO(111)}/I_{LSMO(002)}$, as a function of P_{O_2} (a) and P_{Ar} (b). In (a) P_{Ar} is 0 mbar (black squares), 0.05 mbar (red circles), 0.1 mbar (blue up-pointing triangles), and 0.2 mbar (green down-pointing triangles). Data corresponding to P_{Ar} = 0 mbar are reported in ref. 16. In (b) P_{O_2} is 0.01 mbar (black squares), 0.05 mbar (red circles), and 0.1 mbar (blue up-pointing triangles).

1086 | J. Mater. Chem. C, 2022, **10**, 1084–1089

This journal is © The Royal Society of Chemistry 2022

P_{Ar} pressure (0.1 or 0.2 mbar), the amount of orthorhombic phase only depends slightly on P_{O_2}. In brief, the presence of Ar notably enhances the stabilization of the o-phase for a low P_{O_2} (up to about 0.05 mbar) and does not cause a significant effect for a higher P_{O_2}.

The out-of-plane lattice parameter associated with the HZO(111) reflection, $d_{HZO(111)}$, was determined from the peak position. The dependences of $d_{HZO(111)}$ on P_{O_2} and P_{Ar} are shown in Fig. 3a and b, respectively. The $d_{HZO(111)}$ value expands by decreasing P_{O_2} (Fig. 3a). On the other hand, $d_{HZO(111)}$ of the films deposited at P_{O_2} below around 0.05 mbar depends on P_{Ar}, with $d_{HZO(111)}$ less expanded for a high Ar pressure. The effect of P_{Ar} can be directly visualized in Fig. 3b. The lattice parameter of the films deposited under P_{O_2} = 0.01 mbar (black squares) decrease with increasing P_{Ar} up to 0.1 mbar. The plasma is thermalized for a higher P_{Ar} and $d_{HZO(111)}$ does not change with P_{Ar} or P_{O_2}. To rationalize the intriguing dependence of $d_{HZO(111)}$ on P_{Ar} and P_{O_2} shown in Fig. 3a and b, two causes of cell expansion have to be considered. On one hand, a higher number of oxygen vacancies is expected as P_{O_2} is lower. On the other hand, other point defects can be formed if the PLD plasma has a high energy, which happens when the total pressure, $P_{Ar} + P_{O_2}$, is low. Indeed, deposition under high-energy PLD plasma (low P_{Ar} and low P_{O_2}) reduces strongly the film crystallization (Fig. 1 and 2). Thus, a high oxygen pressure is required to avoid film degradation if P_{Ar} is low. This implies that low oxidation conditions cannot be used to grow HfO$_2$ films when the films are grown using a pure O$_2$ atmosphere. Thus, conventional PLD does not permit growth conditions closer to those that result in the largest ferroelectric polarization when ALD or sputtering is used (low oxidizing conditions).[11] However, as demonstrated here, the use of inert Ar gas to reduce the PLD plasma energy allows the stabilization of the orthorhombic phase with around one order of magnitude lower P_{O_2} (0.01 mbar) than the optimal pressure (0.1 mbar) in conventional PLD (Fig. 2) and importantly reduces the number of defects (signaled by the $d(111)$ expansion, Fig. 3).

Fig. 4a shows the dependence of the leakage current at 1 V on P_{O_2}, for fixed P_{Ar} = 0 mbar (black squares), P_{Ar} = 0.05 mbar (red circles) and P_{Ar} = 0.1 mbar (blue triangles). The corresponding

Fig. 4 (a) Leakage current at 1 V as a function of P_{O_2} for P_{Ar} = 0 mbar (black squares, data reported in ref. 16), P_{Ar} = 0.05 mbar (red circles) and P_{Ar} = 0.1 mbar (blue triangles). (b) Leakage current at 1 V as a function of P_{Ar} for P_{O_2} = 0.01 mbar (black squares), 0.05 mbar (red circles), and 0.1 mbar (blue up-pointing triangles).

leakage–voltage curves can be seen in Fig. S8 (ESI†). The leakage of the films deposited without Ar gas (P_{Ar} = 0 mbar) increases with P_{O_2}, from around 2×10^{-7} A cm^{-2} (P_{O_2} = 0.01 mbar) to 3×10^{-4} A cm^{-2} (P_{O_2} = 0.2 mbar).[16] The films deposited under a mixed O$_2$/Ar atmosphere and a very low P_{O_2} in the 2×10^{-3}–0.01 mbar range are very insulating too, with a leakage current of about 2×10^{-7} A cm^{-2}. In contrast, the film grown under a high total pressure (P_{Ar} = 0.1 mbar and P_{O_2} = 0.1 mbar) is much more conducting. The effect of the total pressure is evident in Fig. 4b, which shows the leakage current at 1 V as a function of P_{Ar} for fixed P_{O_2} = 0.01 mbar (black squares), P_{O_2} = 0.05 mbar (red circles) and P_{O_2} = 0.1 mbar (blue triangles). The leakage current of the three P_{Ar} = 0.05 mbar samples is about 3×10^{-7} A cm^{-2}, without a significant effect of P_{O_2}. However, in the case of the samples grown under a higher P_{Ar}, the leakage is very high when the total pressure ($P_{Ar} + P_{O_2}$) is about 0.2 mbar. Overall, Fig. 4 indicates that a PLD plasma thermalized by a high ambient pressure causes a strong increase in the film conductivity, whereas oxygen vacancies are not the main cause of leakage.

The ferroelectric polarization loops of the films grown under fixed P_{Ar} = 0.05 mbar and varying P_{O_2} are shown in Fig. 5a. The P_{O_2} = 0.01 mbar and 0.02 mbar films have low remanent polarization (P_r) values of 8.3 and 17.1 µC cm^{-2}, respectively. A slightly higher P_{O_2}, 0.05 mbar, results in a high increase of polarization, with P_r = 32 µC cm^{-2}. Further increase of P_{O_2} does not influence significantly the polarization loops, and the P_r of the P_{O_2} = 0.1 mbar film is slightly lower, 30 µC cm^{-2}. The loops of the series of films grown under fixed P_{Ar} = 0.1 mbar are shown in Fig. 5b. In agreement with the presence of the XRD o-HZO(111) reflection in the P_{O2} = 2×10^{-3} and P_{O2} = 5×10^{-3} mbar films, these films exhibit hysteretic polarization loops, with P_r = 13.8 and 18.2 µC cm^{-2}, respectively. The P_r of the films increases with increasing P_{O2}, being 27.8 µC cm^{-2} in the P_{O2} = 0.05 mbar film. The high leakage of the P_{O2} = 0.1 mbar film did not allow the measurement of a loop. The dependence of P_r on P_{O2} is summarized in Fig. 5c for the fixed P_{Ar} = 0 mbar (black squares), P_{Ar} = 0.05 mbar (red circles), P_{Ar} = 0.1 mbar (blue up-pointing triangles) and P_{Ar} = 0.2 mbar (green down-pointing triangle). As described above, the P_r in the P_{Ar} = 0.05 mbar and P_{Ar} = 0.1 mbar films increases with P_{O2}. The same P_{O2}
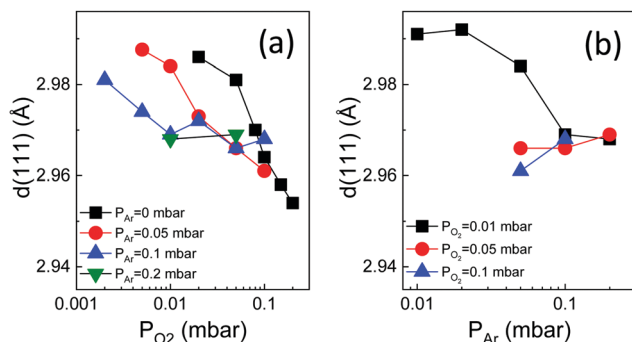

Fig. 3 Out-of-plane lattice parameter, $d_{HZO(111)}$, as a function of P_{O_2} (a) and P_{Ar} (b). In (a) P_{Ar} is 0 mbar (black squares, data reported in ref. 16), 0.05 mbar (red circles), 0.1 mbar (blue up-pointing triangles), and 0.2 mbar (green down-pointing triangles). In (b) P_{O_2} is 0.01 mbar (black squares), 0.05 mbar (red circles), and 0.1 mbar (blue up-pointing triangles).
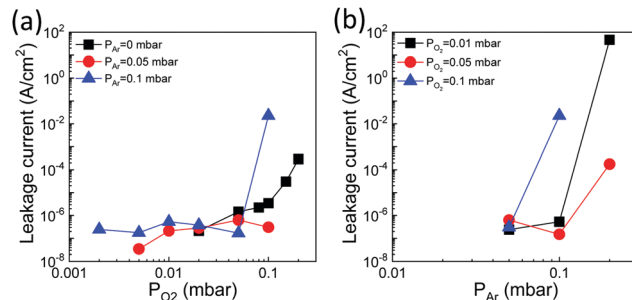
This journal is © The Royal Society of Chemistry 2022
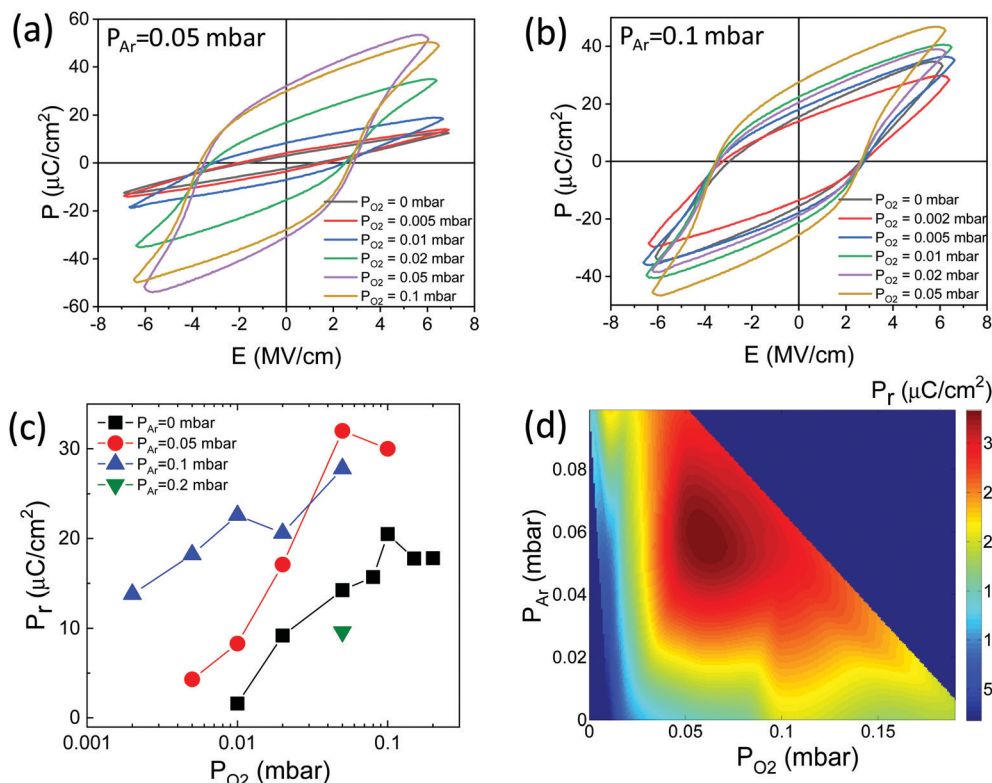
J. Mater. Chem. C, 2022, **10**, 1084–1089 | **1087**

Fig. 5   Ferroelectric polarization loops of the films grown (a) under fixed P_{Ar} = 0.05 mbar and varying P_{O_2} and (b) under fixed P_{Ar} = 0.1 mbar and varying P_{O_2}. (c) Remanent polarization as a function of P_{O_2}, for fixed P_{Ar} = 0 mbar (black squares, data reported in ref. 16), P_{Ar} = 0.05 mbar (red circles), P_{Ar} = 0.1 mbar (blue up-pointing triangles), and 0.2 mbar (green down-pointing triangle). (d) Color map of P_r as a function of P_{Ar} and P_{O_2}. The color map has been constructed after interpolating the data of panel (c) along the P_{Ar} and P_{O_2} axes using cubic splines.

dependence is observed in films grown using conventional PLD (P_{Ar} = 0 mbar).[16] Fig. 5c evidences a huge increase in P_r in the films deposited under a mixed Ar/O$_2$ atmosphere. The highest P_r in the P_{Ar} = 0 mbar series is 20.5 μC cm^{-2} (P_{O_2} = 0.1 mbar film), while it is 32 μC cm^{-2} and 27.8 μC cm^{-2} in the P_{Ar} = 0.05 mbar and P_{Ar} = 0.1 mbar series, respectively, in both cases in films grown under P_{O_2} = 0.05 mbar. Deposition under a higher P_{Ar}, 0.2 mbar, results in P_r reduction. The second benefit of using a mixed Ar/O$_2$ atmosphere is that the films grown under very low P_{O_2} (5 × 10^{-3} mbar in the P_{Ar} = 0.1 mbar series) show high ferroelectric polarization and, as shown in Fig. 4, low leakage, while P_{O_2} above 0.02 mbar is needed in conventional PLD. The color map of P_r as a function of P_{Ar} and P_{O_2} (Fig. 5d) evidences graphically that the optimal conditions to maximize P_r are P_{Ar} = 0.05–0.1 mbar and P_{O_2} around 0.05 mbar. It has to be noted that the measured polarization corresponds to a projection of the ferroelectric dipoles since the films are (111)-oriented. The highest measured P_r = 32 μC cm^{-2} corresponds to a polarization of about 55 μC cm^{-2}, matching well the value of spontaneous polarization calculated for ferroelectric HfO$_2$.[36,37]

critical. Appropriate values of Ar and O$_2$ pressures allow independent control of plasma energy and oxidation conditions during growth. In our study, epitaxial Hf$_{0.5}$Zr$_{0.5}$O$_2$(111) films deposited under a mixed Ar/O$_2$ atmosphere show a low leakage current and have a remanent polarization of about 30 μC cm^{-2}, which represents a 50% increase with respect to equivalent films grown by conventional pulsed laser deposition. Therefore, the simple addition of Ar gas during the growth of the film allows a large increase in ferroelectric polarization, the films probably having the intrinsic polarization of the orthorhombic phase. The new growth process will facilitate the development of epitaxial ferroelectric HfO$_2$ and may be potentially useful in enhancing the properties of polycrystalline HfO$_2$ and other functional oxide and nitride thin films grown by pulsed laser deposition.

Conflicts of interest

There are no conflicts to declare.

4. Conclusions

In summary, in pulsed laser deposition of ferroelectric HfO$_2$ films, a mixed atmosphere of Ar and O$_2$ during growth is

Acknowledgements

1088 | J. Mater. Chem. C, 2022, 10, 1084–1089

This journal is © The Royal Society of Chemistry 2022

References

1 T. S. Böscke, J. Müller, D. Bräuhaus, U. Schröder and U. Böttger, *Appl. Phys. Lett.*, 2011, **99**, 102903.

2 M. H. Park, Y. H. Lee, H. J. Kim, Y. J. Kim, T. Moon, K. Do Kim, J. Müller, A. Kersch, U. Schroeder, T. Mikolajick and C. S. Hwang, *Adv. Mater.*, 2015, **27**, 1811.

3 U. Schröder, C. S. Hwang and H. Funakubo, *Ferroelectricity in Doped Hafnium Oxide: Materials, Properties and Devices*, Woodhead Publishing, 2019.

4 A. Pal, V. K. Narasimhan, S. Weeks, K. Littau, D. Pramanik and T. Chiang, *Appl. Phys. Lett.*, 2017, **110**, 022903.

5 M. Materano, T. Mittmann, P. D. Lomenzo, C. Zhou, J. L. Jones, M. Falkowski, A. Kersch, T. Mikolajick and U. Schroeder, *ACS Appl. Electron. Mater.*, 2020, **2**, 3618.

6 U. Schroeder, M. Materano, T. Mittmann, P. D. Lomenzo, T. Mikolajick and A. Toriumi, *Jpn. J. Appl. Phys.*, 2019, **58**, SL0801.

7 Y. H. Lee, H. J. Kim, T. Moon, K. Do Kim, S. D. Hyun, H. W. Park, Y. Bin Lee, M. H. Park and C. S. Hwang, *Nanotechnology*, 2017, **28**, 305703.

8 T. Mittmann, M. Materano, P. D. Lomenzo, M. H. Park, I. Stolichnov, M. Cavalieri, C. Zhou, C. C. Chung, J. L. Jones, T. Szyjka, M. Müller, A. Kersch, T. Mikolajick and U. Schroeder, *Adv. Mater. Interfaces*, 2019, **6**, 1900042.

9 T. Mittmann, M. Michailow, P. D. Lomenzo, J. Gärtner, M. Falkowski, A. Kersch, T. Mikolajick and U. Schroeder, *Nanoscale*, 2021, **13**, 912.

10 M. H. Park, D. H. Lee, K. Yang, J. Y. Park, G. T. Yu, H. W. Park, M. Materano, T. Mittmann, P. D. Lomenzo, T. Mikolajick, U. Schroeder and C. S. Hwang, *J. Mater. Chem. C*, 2020, **8**, 10526.

11 M. Materano, P. D. Lomenzo, A. Kersch, M. H. Park, T. Mikolajick and U. Schroeder, *Inorg. Chem. Front.*, 2021, **8**, 2650.

12 Y. C. Zhou, Y. K. Zhang, Q. Yang, J. Jiang, P. Fan, M. Liao and Y. C. Zhou, *Comput. Mater. Sci.*, 2019, **167**, 143.

13 I. Fina and F. Sánchez, *ACS Appl. Electron. Mater.*, 2021, **3**, 1530.

14 J. Lyu, I. Fina, R. Solanas, J. Fontcuberta and F. Sánchez, *Appl. Phys. Lett.*, 2018, **113**, 082902.

15 Y. Wei, P. Nukala, M. Salverda, S. Matzen, H. J. Zhao, J. Momand, A. S. Everhardt, G. Agnus, G. R. Blake, P. Lecoeur, B. J. Kooi, J. Íñiguez, B. Dkhil and B. Noheda, *Nat. Mater.*, 2018, **17**, 1095.

16 J. Lyu, I. Fina, R. Solanas, J. Fontcuberta and F. Sánchez, *ACS Appl. Electron. Mater.*, 2019, **1**, 220.

17 Z. Zhang, S. Hsu, V. A. Stoica, H. Paik, E. Parsonnet, A. Qualls, J. Wang, L. Xie, M. Kumari, S. Das, Z. Leng, M. McBriarty, R. Proksch, A. Gruverman, D. G. Schlom, L. Chen, S. Salahuddin, L. W. Martin and R. Ramesh, *Adv. Mater.*, 2021, **33**, 2006089.

18 J. Lyu, I. Fina and F. Sánchez, *Appl. Phys. Lett.*, 2020, **117**, 072901.

19 T. Suzuki, T. Shimizu, T. Mimura, H. Uchida and H. Funakubo, *Jpn. J. Appl. Phys.*, 2018, **57**, 11UF15.

20 S. Amoruso, A. Sambri and X. Wang, *J. Appl. Phys.*, 2006, **100**, 013302.

21 A. Ojeda-G-P, M. Döbeli and T. Lippert, *Adv. Mater. Interfaces*, 2018, **5**, 1701062.

22 J. Gonzalo, C. N. Afonso and J. Perrière, *Appl. Phys. Lett.*, 1995, **67**, 1325.

23 C. B. Arnold and M. J. Aziz, *Appl. Phys. A: Mater. Sci. Process.*, 1999, **69**, S23.

24 S. Wicklein, A. Sambri, S. Amoruso, X. Wang, R. Bruzzese, A. Koehl and R. Dittmann, *Appl. Phys. Lett.*, 2012, **101**, 131601.

25 C. Xu, S. Wicklein, A. Sambri, S. Amoruso, M. Moors and R. Dittmann, *J. Phys. D: Appl. Phys.*, 2014, **47**, 034009.

26 P. R. Willmott, R. Herger, C. M. Schlepütz, D. Martoccia and B. D. Patterson, *Phys. Rev. Lett.*, 2006, **96**, 176102.

27 B. Shin and M. J. Aziz, *Phys. Rev. B: Condens. Matter Mater. Phys.*, 2007, **76**, 085431.

28 C. S. Ma, S. K. Hau, K. H. Wong, P. W. Chan and C. L. Choy, *Appl. Phys. Lett.*, 1996, **69**, 2030.

29 T. Scharf and H. U. Krebs, *Appl. Phys. A: Mater. Sci. Process.*, 2002, **75**, 551.

30 J. Gonzalo, J. Siegel, A. Perea, D. Puerto, V. Resta, M. Galvan-Sosa and C. N. Afonso, *Phys. Rev. B: Condens. Matter Mater. Phys.*, 2007, **76**, 035435.

31 N. B. Ibrahim, C. Edwards and S. B. Palmer, *J. Magn. Magn. Mater.*, 2000, **220**, 183.

32 S. B. Ogale, R. Nawathey-Dikshit, S. J. Dikshit and S. M. Kanetkar, *J. Appl. Phys.*, 1992, **71**, 5718.

33 J. Wang, G. Rijnders and G. Koster, *Appl. Phys. Lett.*, 2018, **113**, 223103.

34 M. Mirjolet, F. Sánchez and J. Fontcuberta, *Adv. Funct. Mater.*, 2019, **29**, 1808432.

35 P. Nukala, J. Antoja-Lleonart, Y. Wei, L. Yedra, B. Dkhil and B. Noheda, *ACS Appl. Electron. Mater.*, 2019, **1**, 2585.

36 T. D. Huan, V. Sharma, G. A. Rossetti and R. Ramprasad, *Phys. Rev. B: Condens. Matter Mater. Phys.*, 2014, **90**, 064111.

37 F. Delodovici, P. Barone and S. Picozzi, *Phys. Rev. Mater.*, 2021, **5**, 064405.

This journal is © The Royal Society of Chemistry 2022

J. Mater. Chem. C, 2022, **10**, 1084–1089 | **1089**